ELSEVIER

Tectonophysics 351 (2002) 331–341

TECTONOPHYSICS

www.elsevier.com/locate/tecto

A scanning electron microscope study of the effects of dynamic recrystallization on lattice preferred orientation in olivine

Kyung-Ho Lee, Zhenting Jiang[1], Shun-ichiro Karato*,[1]

Department of Geology and Geophysics, University of Minnesota, Minneapolis, MN 55455, USA

Received 5 January 2001; received in revised form 24 January 2002; accepted 3 May 2002

Abstract

Effects of dynamic recrystallization on lattice preferred orientation (LPO) in olivine were investigated through the combination of two SEM-based techniques, electron backscattered diffraction (EBSD) technique for crystallographic orientation measurement and backscattered electron imaging (BEI) for dislocation observation. Samples are experimentally deformed olivine aggregates in simple shear geometry. In the sample deformed at $T = 1473$ K and high stresses (~ 480 MPa), only incipient dynamic recrystallization is observed along grain-boundaries. Orientations of these small recrystallized grains are more random than that of relict grains, suggesting an important role of grain-boundary sliding at this stage of recrystallization. In the sample deformed at $T = 1573$ K and low stress (~ 160 MPa), dynamic recrystallization is nearly complete and the LPO is characterized by two [100] peaks. One peak is located at the orientation subparallel to the shear direction and is dominated by grains with high Schmid factor. The other occurs at high angles to the shear direction and is due to the contribution from grains with low Schmid factor. Grains with high Schmid factor tend to have higher dislocation densities than those with low Schmid factor. Based on these observations, we identify two mechanisms by which dynamic recrystallization affects LPO: (1) enhancement of grain-boundary sliding due to grain-size reduction, leading to the modification of LPO caused by the relaxation of constraint for deformation; (2) grain-boundary migration by which grains with lower dislocation densities grow at the expense of grains with higher dislocation densities. Based on the deformation mechanism maps and stress versus recrystallized grain-size relation, we suggest that the first mechanism always plays an important role whereas the second mechanism has an important effect only under limited conditions.

Keywords: Dynamic recrystallization; Olivine; Lattice preferred orientation; EBSD; SEM

1. Introduction

Lattice preferred orientation (LPO or fabric) could develop either through the rotation of crystallographic axis during dislocation creep or twinning (e.g., van Houte and Wagner, 1985) or by recrystallization (e.g., Gottstein and Mecking, 1985; Doherty et al., 1997). Although the mechanisms of LPO development due to deformation-induced lattice rotation are well understood, including cases where the number of available slip systems is small (e.g., Molinari et al., 1987; Ribe and Yu, 1991; Wenk et al., 1991), the mechanisms of LPO development during recrystallization, particularly dynamic recrystallization, are poorly understood (Lister and Price, 1978; Green et al., 1970; Gottstein

* Corresponding author. Department of Geology and Geophysics, Yale University, 109 Kline Geology Laboratory, P.O. Box 208109E, New Haven, CT 06520-8109, USA. Fax:+1-203-432-3134.

E-mail address: shun-ichiro.karato@yale.edu (S. Karato).

[1] Now at Department of Geology and Geophysics, Yale University, New Haven, CT 06520, USA.

0040-1951/02/$ - see front matter
PII: S0040-1951(02)00250-0

and Mecking, 1985; Urai et al., 1986; Karato, 1987a, 1988; Jessel, 1988a,b; Gleason et al., 1993; Wenk et al., 1997; Doherty et al., 1997; Wenk and Tomé, 1999; Kaminski and Ribe, 2001).

Two processes could affect the LPO development during dynamic recrystallization. Firstly, small grains formed by dynamic recrystallization may relax the constraints for deformation of grains and hence the number of slip systems activated will be reduced, which could lead to a change in LPO. Secondly, dynamic recrystallization sometimes involves strain-induced grain-boundary migration. Grains with low dislocation densities will grow by consuming grains with high dislocation densities. When orientation dependence of dislocation density is strong, this process leads to a new type of LPO.

Consequently, the key to understand the way in which dynamic recrystallization affects LPO is the microstructures, such as dislocation distribution and its relation to crystallographic orientation as well as size and morphology of grains. An earlier study by Karato (1987a, 1988) investigated the dislocation structures using backscattered electron imaging (BEI) technique (Karato, 1987b), but the orientation measurements were made using an optical microscope with poor spatial resolution. Zhang et al. (2000) measured LPO of olivine aggregates using electron backscattered diffraction (EBSD) technique (Dingley and Randle, 1992; Adams et al., 1993), but the dislocation structures were not investigated in any detail. The main purpose of this study is to extend these previous studies by combining these two high-resolution SEM-based techniques in order to improve our understanding of the role of dynamic recrystallization in the development of LPO.

2. Samples

A large number of simple shear deformation experiments on olivine aggregates were carried out by Karato's group using a gas-medium, high-pressure and temperature apparatus. Among them, samples of two series of experiment conducted at 1473 and 1573 K, respectively, show distinct difference in microstructural and textural development (Zhang et al., 2000). Samples deformed at $T = 1473$ K and relatively high stress (300–500 MPa) showed small degree of recrystallization (10–20%) and most of the original grains show large elongation. We call this type of microstructure as H-type microstructure. On the other hand, samples deformed at 1573 K and relatively low stress (130–200 MPa) show higher degree of dynamic recrystallization and grain-shape is nearly equant, we call this, L-type microstructure. We selected one representative sample from each group, PI-284 from H-type and MIT-23 from L-type (Table 1). PI-284 was deformed at a constant strain rate of 9.5×10^{-5} s^{-1} and temperature 1473 K to a final strain of 120%. The deviatoric stress kept increasing and the final value was $\sim$ 478 MPa. The deformation of MIT-23 was carried out at nearly the same strain rate as PI-284, but at a higher temperature (1573 K). The sample shows a peak strength $\sim$ 150 MPa at $\sim$ 40% strain and a slight strain hardening thereafter. The final strain of this sample is $\sim$ 140% at maximum stress of $\sim$ 160 MPa. For more details of deformation experiments, see Zhang et al. (2000).

Table 1
Conditions for deformation experiments (Zhang et al., 2000)

Sample	T (K)	γ	σ_{max} (MPa)[a]	$\dot{\gamma}$ (s^{-1})[b]	d_i (μm)[c]	d_f (μm)[d]
PI-284	1473	1.10	478	9.6×10^{-5}	37	2–35
MIT-23	1573	1.43	160	9.5×10^{-5}	34	10

[a] Maximum stress ($\sigma_1 - \sigma_3$).
[b] Shear strain rate.
[c] Initial grain-size.
[d] Final grain-size (in PI-284, grain-size is bi-modal).

3. Experimental techniques

3.1. Dislocation density measurement

Dislocations and grain-boundaries were observed on decorated samples using BEI (Karato, 1987b). This technique allows to investigate dislocation structures over whole sample area with a spatial resolution of to $\sim$ 0.1 μm. Decoration was made in air at $T = 1073$ K for 1 h. The sample surface was then gently polished to remove a thin layer of oxides. The work was carried out on JEOL 840A SEM located in University of Minnesota, operated at 15 kV accelerating voltage, 10 nA probe current and 8 mm working distance. A number of 5×5 or 10×10 μm^2 windows or irregular

shape windows out of each grain were used to measure the dislocation density from backscattered electron images where dislocation density is defined as:

$$\rho \equiv \sum l/V \quad (1)$$

where ρ is the dislocation density and Σl is the total length of dislocations in a volume V (see Karato and Lee, 1999).

3.2. Crystallographic orientation measurement

EBSD technique was employed to determine crystallographic orientation (Dingley and Randle, 1992; Adams et al., 1993; Prior et al., 1999). The work was carried out on JEOL 840 SEM customized with HKL's EBSD system at the University of Minnesota. The spatial resolution of this system is about 1 μm. All EBSD patterns were manually indexed using HKL's Channel4 software package. The bulk LPO was collected randomly at fixed step with step size varied according to grain size, whereas LPO of specified grain groups, such as small or large grains (Sample PI-284) and grains with different dislocation density, were measured separately. The samples for EBSD measurement were mechanically polished. They were then polished using colloidal silica as suspension to remove the surface damage and coated with a thin carbon-layer (about 3 nm). The sample was mounted onto a stage whose top surface is inclined with 20° to the electron beam. The SEM was operated under 30 kV accelerating voltage, 10 nA beam current and 25 mm working distance.

4. Results

4.1. Grain and dislocation structures

4.1.1. Sample PI-284 (H-type)

Sample PI-284 shows typical core–mantle structures with elongated original grains (old grains) as cores rimmed by small grains derived from dynamic recrystallization (Fig. 1a). These microstructures are similar to that of deformed quartzite in regime II (Hirth and Tullis, 1992), suggesting that progressive subgrain rotation is the dominant mechanism of recrystallization in this regime. The elongated original grains contain a number of sub-boundaries and subgrain formation is more pronounced at the margins of the old grains than at their centers (Fig. 1a). The small grains are mainly developed along old grain boundaries, forming zones with the width of $\sim 1/5$ of the size of original grains and occupied less than 10% of the total volume (Fig. 1a). Dynamic recrystallization also occurs along some shear bands. These new grains with the grain-size around 1–3 μm have nearly equiaxed grain-shape (Fig. 1b) and in most cases their boundaries assume near equilibrium morphology, but non-equilibrium morphology, such as four-grain junctions, is often seen (pointed by arrows in Fig. 1b).

Dislocation distribution is heterogeneous. Dislocation densities in large original grains are generally higher than those of new grains. In fact, new grains near the boundaries of large grains are generally dislocation-free (Fig. 1b). Measurements of dislocation density are performed on 83 grains. The result shows that the dislocation density varies in the range of 0 to $\sim 50\ \mu m^{-2}$.

4.1.2. Sample MIT-23 (L-type)

In sample MIT-23, dynamic recrystallization is much more extensive and almost all regions are replaced by new grains (Fig. 1c). The grain structure is characterized by nearly equiaxed to slightly elongated grain-shape and the average shape of grains does not reflect overall strain of the sample. These features are comparable with that of deformed quartz in regime III (Hirth and Tullis, 1992), suggesting that both subgrain rotation and grain-boundary migration are responsible for microstructural development in this regime. The grain-size varies from 2 to 15 μm with the mean size around 5–8 μm.

Dislocation distribution in sample MIT-23 is also highly heterogeneous (Fig. 1d). Measurements on 157 grains show that dislocation density ranged from 1 to $45\ \mu m^{-2}$. Generally, there exists a correlation between grain-boundary morphology and dislocation density. Grains with low dislocation densities (or portions of grains with low dislocation densities) tend to have convex outward grain-boundary morphology whereas grains with high dislocation densities (or portions of grains with high dislocation densities) have concave outward grain-boundary morphology (Fig. 1d), suggesting that the grains with low dislocation density are growing while grains with high dislocation density are shrinking.

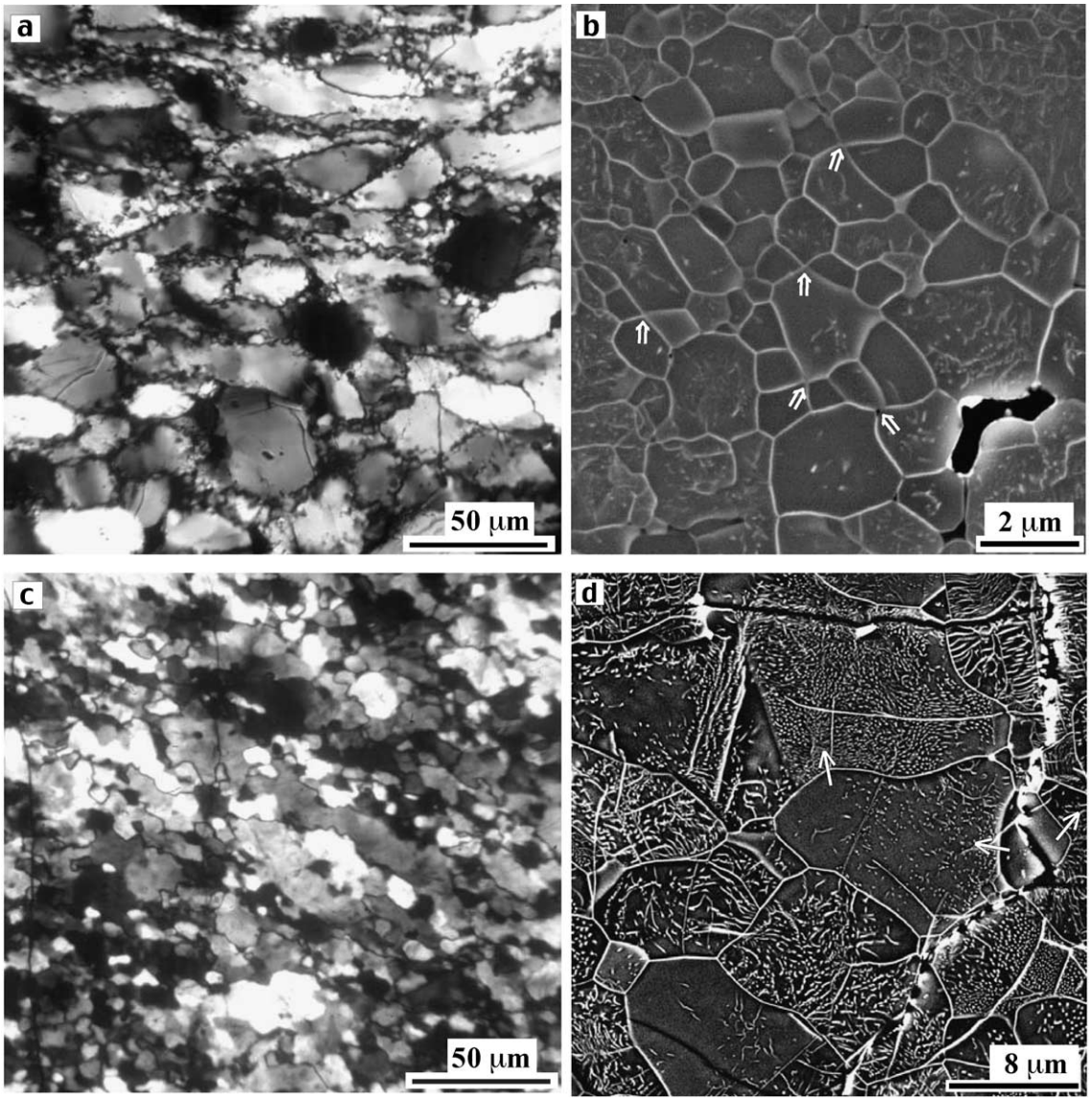

Fig. 1. Microstructures of olivine aggregates deformed by simple shear. The starting materials are hot-pressed aggregates with nearly equilibrium grain morphology (grain size is 34–37 μm). (a) An optical micrograph of PI-284, showing typical core–mantle structures. (b) A close-up BEI micrograph of sample PI-284 from a region near grain-boundary, showing a large number of dynamically recrystallized grains with four-grain junctions (shown by arrows) which suggest extensive grain-boundary sliding (or grain switching events). (c) An optical micrograph of sample MIT-23 showing nearly complete recrystallization. (d) A BEI micrograph of sample MIT-23. Note the heterogeneity in dislocation densities and corresponding variation in grain-boundary morphology. All images are taken from *XZ* section with *X* parallel to the horizontal edge. *X* = Shear direction; *Z* = shear plane normal. (a)+(c) are taken under crossed nicole.

4.2. Lattice preferred orientation (LPO)

Microstructural observations show that dislocation density is heterogeneous and grain-boundary morphology is also variable. Therefore, LPO was not only measured for overall samples, but also measured separately for grains with different microstructural characteristics in order to investigate the role of

microstructural heterogeneity in the development of LPO. Two different microstructural characteristics were used to classify grains. First, grains were grouped in terms of dislocation density: high-density grains (top 30%), low-density grains (bottom 30%) and intermediate-density grains (middle 40%). Second, grains were also classified due to grain size (H-type sample).

4.2.1. Sample PI-284

The bulk LPO of this sample is shown in Fig. 2a. The peak of [100] axes is strong and oriented close to the shear direction. The [001] axes form a less pronounced peak sub-parallel to the shear direction and a weak girdle perpendicular to the shear plane. The poles of (010) form two clusters within a girdle normal to the shear plane.

The LPOs of different grains are grouped according to the dislocation density and are displayed in Fig. 2b–d. Grains of high dislocation density (12–50 μm^{-2}) show a strong [100] peak close to the shear direction with the peak of [010] around the pole of the shear (Fig. 2b), indicating that these grains are

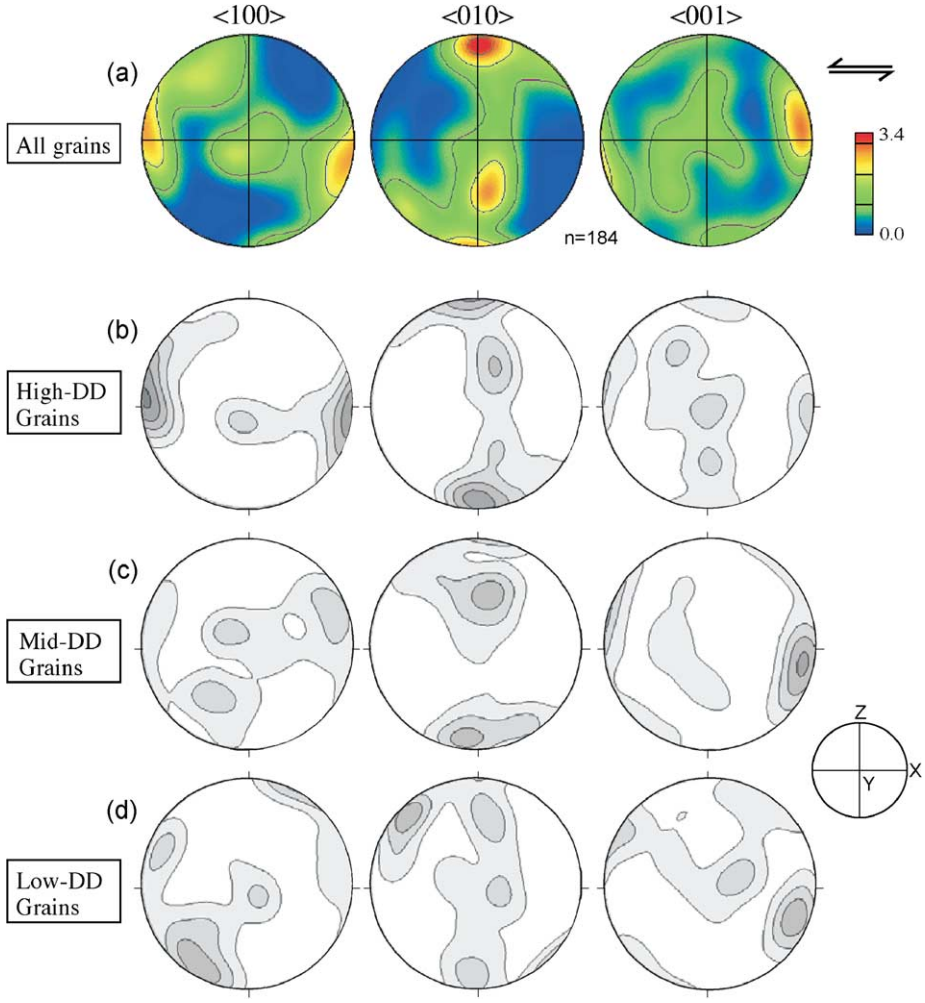

Fig. 2. LPOs of sample PI-284, showing contours of density of poles in the lower-hemisphere equal-area stereographic projection. The density of poles is relative to the uniform distribution. (a) Pole figures of bulk sample; (b) pole figures of grains with high dislocation density (DD) (upper 30%); (c) intermediate dislocation density (middle 40%) and (d) low dislocation density (lower 30%). The projection of the sample coordinate (*X*, *Y* and *Z*) is given by an insert figure.

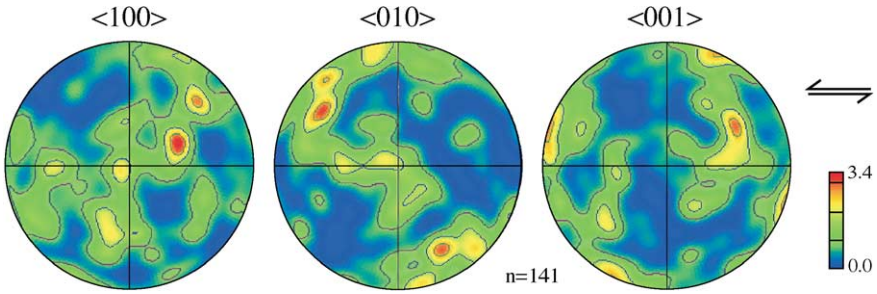

Fig. 3. LPO of small grains in Sample PI-284. See Fig. 2 for the reference for plotting. Lower hemisphere equal area projection.

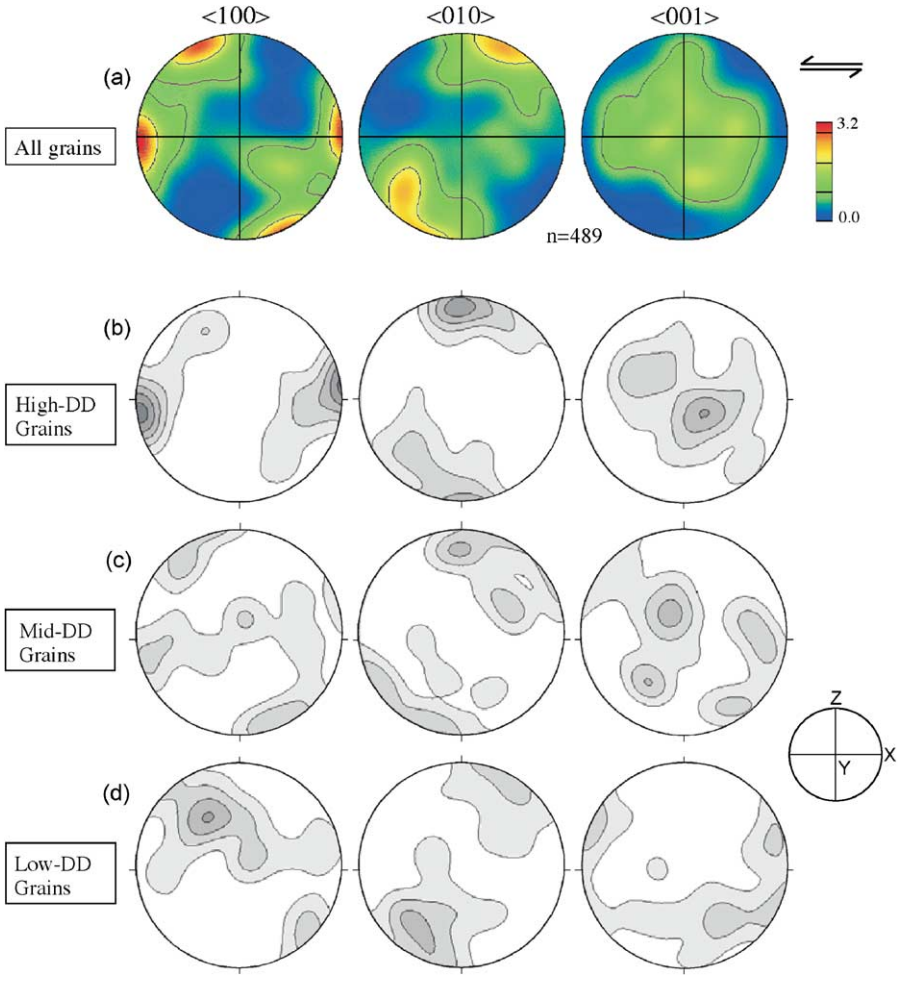

Fig. 4. LPOs of sample MIT-23, showing contours of density of poles in the lower-hemisphere equal area stereographic projection. The density of poles is relative to the uniform distribution. (a) Pole figures of bulk sample; (b) pole figures of grains with high dislocation density (upper 30%); (c) intermediate dislocation density (middle 40%) and (d) low dislocation density (lower 30%). The projection of the sample coordinate (*X*, *Y* and *Z*) is given by an insert figure. Lower hemisphere equal area projection.

deformed predominantly by dislocation glide on the [100] (010) slip system. Grains with low and medium dislocation densities have modest peaks of [100] and [001] axes at high angles with respect to the shear direction. The [001] peaks seem stronger for grains with low to intermediate dislocation densities (Fig. 5c–d) in comparing with that of grain of high dislocation density.

The data measured from small grains throughout the sample are plotted in Fig. 3. The measurements were made for small grains that are associated with a large number of original grains in order to minimize the bias caused by the orientation of large (parent) grains. LPOs of small grains are weaker in comparing to that of the bulk sample (Fig. 2a). Considering that small grains occupy less than 15% of the total sample volume, they do not make a significant contribution to the bulk LPO of the sample.

4.2.2. Sample MIT-23

The LPO of this sample is characterized by dual peaks of [100]. One is nearly parallel to the shear direction and the other weaker one is inclined at $\sim 60^\circ$ to the shear direction (Fig. 4a). The [001] axes do not form a peak close to the shear direction as they do in Sample PI-284, but scattered around the direction perpendicular to both the shear direction and shear plane normal. The peak of [010] is sub-parallel to the pole of the shear plane.

LPOs of grains of high dislocation density (14.5–43 μm^{-2}) are comparable to that of grains of high dislocation density group in sample PI-284 and are very close to the single crystal orientation with the peak of [100] parallel to the shear direction, [010] peak close to the pole of shear plane and [001] axes around the direction parallel to the shear plane and normal to the shear direction (Fig. 4b). It is consistent with the easy slip on the [100](010) slip system. Grains with low dislocation density (<4.0 μm^{-2}) display a relatively weak LPO in comparing to grains of high dislocation density group. Most of the [100] axes are scattered in a plane inclined at 45° to the shear plane and that of [010] axes form a peak close to the periphery at an angle of 30° to the pole of the shear plane (Fig. 4d). Grains of medium dislocation density group (4.0–14.5 μm^{-2}) contain fabric components from both low and high dislocation density groups (Fig. 4c). Comparing the bulk LPO with that of three different grain groups, it is evident that the dual peaks of [100] of bulk sample are related to grains with different dislocation densities. The [100] peak close to the shear direction is clearly contributed by grains with high dislocation density, while the other peak, inclined at $\sim 45^\circ$ to the shear direction, is formed by grains of low and medium dislocation density.

5. Discussions

5.1. Effects of grain-size reduction

Effects of grain-size reduction can be most clearly investigated for H-type samples where grain-size distribution is bimodal (Fig. 1a). Microstructural observations suggest that small grains are formed as a result of dynamic recrystallization. The LPO of small-recrystallized grains in PI-284 is significantly weaker than that of original grains (comparing Fig. 2a with Fig. 3). Moreover, a large number of four-grain junctions (Fig. 1b) indicate active grain switching events (or grain-boundary sliding) (Ashby and Verrall, 1973). Furthermore, many of the small grains in H-type samples are dislocation-free and their morphology shows near equilibrium geometry (Fig. 1b). These observations strongly suggest that small grains in H-type samples are deformed by diffusional creep or grain-boundary sliding. This conclusion is supported by the deformation mechanism maps (Fig. 5), showing that stress/grain-size conditions for small-recrystallized grains in H-type samples are well in the diffusional creep regime.

This implies that deformation occurs by a combination of dislocation and diffusion creep (or grain-boundary sliding) when dynamic recrystallization occurs. When these grain-size-sensitive deformation mechanisms make a significant contribution to total strain, then the constraints on deformation, such as the von Mises condition, can be relaxed. This will lead to a change in the mechanisms of deformation from multi-slip regime in coarse-grained samples to single-slip regime in small-grained samples as suggested by Drury and Fitz Gerald (1998). Consequently, dynamic recrystallization will strengthen and/or simplifies LPO in olivine so that a "single-slip" LPO may be realized by this mechanism. This provides an

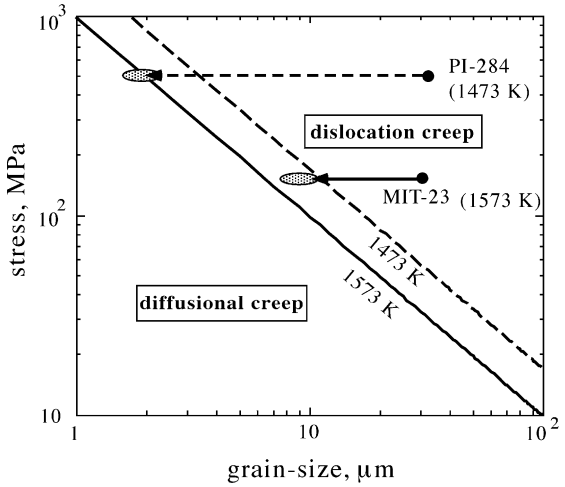

Fig. 5. A deformation mechanism map of olivine (after Karato et al., 1986) with grain-size stress conditions of the samples used in this study. Solid circles represent the initial grain-size and the hatched ellipsoids show recrystallized grain-size. In the sample PI-284, only a small fraction of the sample was recrystallized, and these regions fall in the diffusion creep regime whereas the majority of the sample remains in the dislocation creep regime. In contrast, in the sample MIT-23, recrystallization is nearly complete and the final grain-size is close to the boundary between diffusional creep and dislocation creep regimes, but still in the dislocation creep regime.

explanation for the fast rotation of [100] peak towards shear direction after significant dynamic recrystallization as observed by Zhang and Karato (1995) and Zhang et al. (2000).

5.2. Effects of grain-boundary migration

Effects of grain-boundary migration can be identified by correlating dislocation density with grain-boundary morphology and grain size (e.g., Fig. 1d). We often observe curved boundaries between two grains with largely different dislocation density in which dislocation density is lower in a grain toward the center of curvature than that in the other grain. In these cases, we infer that the boundary is likely to have been migrating caused by the heterogeneity in dislocation density (Karato, 1989a). Such features are commonly observed in L-type samples (Fig. 1d), but less pronounced in H-type samples. Therefore, we will discuss the effects of grain-boundary migration only in reference to the observations in L-type samples.

The dual [100] peaks in LPOs of L-type sample (Fig. 4) are due to the contribution of grains from two different groups. While the first peak sub-parallel to

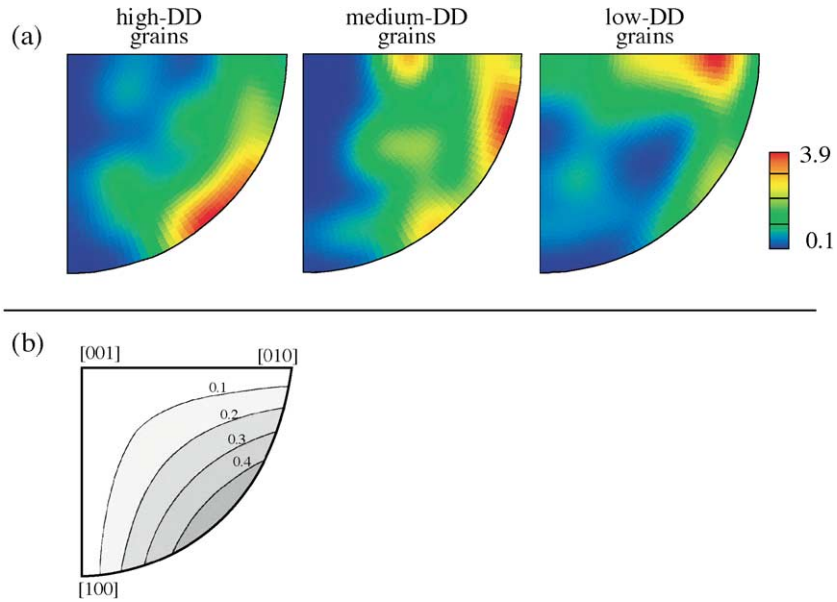

Fig. 6. (a) Inverse pole figures (generated by plotting the orientation of principal compressive stress (σ_1) into the crystallographic coordinate) showing distribution of σ_1 for grains of three different dislocation density (DD) groups. (b) Contour map of Schmid factor in crystallographic coordinate calculated for the [100](010) slip system of olivine.

the shear direction is predominantly formed by grains with high dislocation density and concave outward grain-boundary morphology, the second peak corresponds to grains with low dislocation density and convex outward boundaries. As grains of low dislocation density are likely growing by consuming grain of high dislocation density, it is reasonable to suggest that formation of secondary [100] peak is due to strain-induced grain-boundary migration.

To better understand the processes by which grain boundary migration modifies LPO, we have investigated the correlation between dislocation density and crystal orientation and the relationship between the Schmid factor and dislocation density as shown in Fig. 6a–b. The inverse pole figures (IPFs) in Fig. 6a are generated by plotting the principal compressive stress (σ_1) in to the crystallographic coordinate of each grain belonging to different dislocation density. Fig. 6b shows a contour map of a Schmid factor calculated for the [100](010) slip system on a crystallographic coordinate as a function of orientation of principal compressive stress. We can clearly see the following trend: the grains with high dislocation densities have crystallographic orientations with high Schmid factor for the [100](010) slip system while the grains with low dislocation densities have orientations with low Schmid factor for the same slip system. Such a dependence of dislocation density on crystallographic orientation leads to selective growth of grains with low Schmid factors, resulting in a significant modification to LPO.

6. Summary

Two important processes have been identified by which dynamic recrystallization modifies LPO in olivine. First, grain-size reduction caused by dynamic recrystallization enhances the contribution from grain-size sensitive flow to total strain and modifies LPO. We suggest that this will reduce the number of slip systems needed for deformation of a polycrystalline aggregate and strengthen LPO and rotate it toward the "single-slip LPO." According to the deformation mechanism maps (Karato et al., 1986) and the stress versus dynamically recrystallized grain-size (Karato et al., 1980) in olivine, the contribution from grain-size sensitive creep is significant under most of experimental and natural deformation conditions (see also Drury and Fitz Gerald, 1998).

Second, we have clear evidence for modification of LPO by grain-boundary migration. Grain-boundary migration results in the secondary peak at the orientation corresponding to the low Schmid factor for the dominant slip system. However, the degree to which this process modifies the LPO is likely to depend on the degree of heterogeneity in dislocation density and the rate of boundary migration relative to the rate of rotation of orientation due to deformation (e.g., Karato, 1987a). The present results show that the contribution from the primary and the secondary peak is roughly equal under the experimental conditions, which is consistent with the model by Karato (1987a). Relatively low temperatures may favor the contribution of grain-boundary migration, but the heterogeneity in dislocation density will be low under high stress conditions and low temperatures because of the operation of multi-slip systems.

Some modeling studies addressed the role of dynamic recrystallization on LPO development in olivine (Wenk and Tomé, 1999; Kaminski and Ribe, 2001). Both of these studies suggested that the observed rapid rotation of peaks in pole figures is due to "oriented nucleation." They considered that nucleation of new grains occurs selectively from grains with high Schmid factors and they grow, without changing their orientations, to dominate the LPO. Some of our results are not quite consistent with these models. Firstly, their models imply that grains with high Schmid factors should have highly heterogeneous dislocation density: grains prior to recrystallization should have high dislocation density whereas newly recrystallized grains should have very low dislocation density. However, the present results show that grains with high Schmid factors are dominated by those with high dislocation density (Fig. 6). Secondly, grains with high Schmid factor are, by definition, easy to deform. Therefore, dislocation densities of those grains should soon become high and they will stop growing. We consider that although nucleation likely occurs in highly deformed grains, grains that grow and significantly modify LPO are those which have largely different orientations from their parent grains: grain orientations in these highly deformed regions are largely modified by subgrain-rotation, and among many grains with different orientations, those with

low Schmid factors will selectively grow. In short, our observations suggest the importance of ''oriented (selected) growth'' in LPO development associated with dynamic recrystallization.

Bystricky et al. (2000) performed large strain simple shear deformation experiments on olivine aggregates under the conditions nearly identical to that of experiment PI-284 (H-type). The LPO of their samples at similar strains is much the same as ours, but LPO appears to evolve with strains. At larger strains LPO is characterized by a strong peak of [100] parallel to the shear direction and [001] and [010] axes define a girdle. The contribution from ***b***=[001] slip appears to decrease with strain due presumably to the relaxation of constraints on deformation by grain-size reduction.

Finally, we emphasize that the present results are on samples that contain relatively small amount of water. Recent studies in our lab indicate that water has profound effects on LPO development in olivine and the kinetics of dynamic recrystallization (Jung and Karato, 2001a,b). Therefore, the role of dynamic recrystallization under water-rich conditions may be substantially different from that under water-poor conditions.

Acknowledgements

We thank Shuqing Zhang who performed most of the deformation experiments. Detailed comments by two reviewers, David Prior and Jan Tullis, greatly helped improve this paper. Discussions with John Fitz Gerald, Martyn Drury and Shuqing Zhang and technical assistance by Stuart McKernan at High-Resolution Microscopy Center at University of Minnesota are gratefully acknowledged. This research was supported by NSF (EAR–9903087).

References

Adams, B.L., Wright, S.I., Kunze, K., 1993. Orientation imaging: the emergence of a new microscopy. Metall. Trans. 23A, 819–831.

Ashby, M.F., Verrall, R.A., 1973. Diffusion-accommodated flow and superplasticity. Metall. Trans. 21, 149–1163.

Bystricky, M., Kunze, K., Burlini, L., Burg, J.-P., 2000. High shear strain of olivine aggregates: rheological and seismic consequences. Science 290, 1564–1567.

Dingley, D.J., Randle, V., 1992. Microtexture determination by electron back-scatter diffraction. J. Mater. Sci. 27, 4545–4566.

Doherty, R.D., Hughes, D.A., Humphreys, F.J., Jonas, J.J., Jensen, D.J., Kassner, M.E., King, W.E., McNelley, T.R., McQueen, H.J., Rollett, A.D., 1997. Current issues in recrystallization: a review. Mater. Sci. Eng. A238, 219–274.

Drury, M.R., Fitz Gerald, J.D., 1998. Mantle rheology: insights from laboratory studies of deformation and phase transition. In: Jackson, I. (Ed.), The Earth's Mantle. Cambridge Univ. Press, Cambridge, pp. 503–559.

Gleason, G.C., Tullis, J., Heidelbach, F., 1993. The role of dynamic recrystallization in the development of lattice preferred orientations in experimentally deformed quartz aggregates. J. Struct. Geol. 15, 1145–1168.

Gottstein, G., Mecking, H., 1985. Recrystallization. In: Wenk, H.-R. (Ed.), Preferred Orientation in Deformed Metals and Rocks: Introduction to Modern Texture Analysis. Academic Press, San Diego, pp. 183–218.

Green, H.W., Griggs, D.T., Christie, J.M., 1970. Syntectonic and annealing recrystallization of fine-grained quartz aggregates. In: Paulitsch, P. (Ed.), Experimental and Natural Rock Deformation. Springer, Berlin, pp. 272–335.

Hirth, G., Tullis, J., 1992. Dislocation creep regimes in quartz aggregates. J. Struct. Geol. 14, 145–159.

Jessel, M.W., 1988a. Simulation of fabric development in recrystallizing aggregates—I. Description of the model. J. Struct. Geol. 10, 771–778.

Jessel, M.W., 1988b. Simulation of fabric development in recrystallizing aggregates—II. Example model runs. J. Struct. Geol. 10, 779–793.

Jung, H., Karato, S., 2001a. Effects of water on dynamically recrystallized grain-size of olivine. J. Struct. Geol. 23, 1337–1344.

Jung, H., Karato, S., 2001b. Water induced fabric transitions in olivine. Science 293, 1460–1463.

Kaminski, E., Ribe, N.M., 2001. A kinematic model for recrystallization and texture development in olivine polycrystals. Earth Planet. Sci. Lett. 189, 253–267.

Karato, S., 1987a. Seismic anisotropy due to lattice preferred orientation in minerals: kinematic or dynamic? In: Manghnani, M.H., Syono, Y. (Eds.), High-Pressure Research in Mineral Physics. TERRAPUB/AGU, Tokyo, pp. 455–471.

Karato, S., 1987b. Scanning electron microscope observation of dislocations in olivine. Phys. Chem. Miner. 14, 245–248.

Karato, S., 1988. The role of recrystallization in the preferred orientation of olivine. Phys. Earth Planet. Inter. 51, 107–122.

Karato, S., 1989a. Seismic anisotropy: mechanisms and tectonic implications. In: Karato, S., Toriumi, M. (Eds.), Rheology of Solids and of the Earth. Oxford Univ. Press, Oxford, pp. 393–422.

Karato, S., Lee, K.-H., 1999. Stress-strain distribution in deformed olivine aggregates: inference from microstructural observations and implications for texture development. In: Szpunar, J.A. (Ed.), Proceedings of the 12th International Conference on Textures of Materials. Natl. Res. Counc. Press, Ottawa, pp. 1546–1555.

Karato, S., Toriumi, M., Fujii, T., 1980. Dynamic recrystallization in olivine during high temperature creep. Geophys. Res. Lett. 7, 649–652.

Karato, S., Paterson, M.S., Fitz Gerald, J.D., 1986. Rheology of synthetic olivine aggregates: influence of grain size and water. J. Geophys. Res. 91, 8151–8176.

Lister, G.S., Price, G.P., 1978. Fabric development in a quartz-feldspar mylonite. Tectonophysics 49, 37–78.

Molinari, A., Canova, G.R., Wenk, H.-R., 1987. A self-consistent approach of the large deformation polycrystal viscoplasticity. Acta Metall. 35, 2983–2994.

Prior, D.J., Boyle, A.P., Brenker, F., Cheadle, M.C., Day, A., Lopez, G., Peruzzo, L., Potts, G.J., Reddy, S., Spiess, R., Timms, N.E., Trimby, P., Wheeler, J., Zetterström, L., 1999. The application of electron backscatter diffraction and orientation imaging in the SEM to textural problems in rocks. Am. Mineral. 84, 1741–1759.

Ribe, N.M., Yu, Y., 1991. A theory of plastic deformation and textural evolution of olivine polycrystals. J. Geophys. Res. 96, 8325–8335.

Urai, J.L., Means, W.D., Lister, G.S., 1986. Dynamic recrystallization of minerals. In: Hobbs, B.E., Heard, H.C. (Eds.), Mineral and Rock Deformation: Laboratory Studies. Am. Geophys. Union, Washington, DC, pp. 161–199.

van Houte, P., Wagner, F., 1985. Development of texture by slip and twinning. In: Wenk, H.-R. (Ed.), Preferred Orientation in Deformed Metals and Rocks: Introduction to Modern Texture Analysis. Academic Press, San Diego, pp. 233–258.

Wenk, H.-R., Tomé, C.N., 1999. Modeling dynamic recrystallization of olivine aggregates deformed in simple shear. J. Geophys. Res. 104, 25, 513–25, 527.

Wenk, H.-R., Bennett, K., Canova, G., Molinari, A., 1991. Modeling plastic deformation of peridotite with the self-consistent theory. J. Geophys. Res. 96, 8337–8349.

Wenk, H.-R., Canova, G., Bréchet, Y., Flandin, L., 1997. A deformation-based model for recrystallization of anisotropic materials. Acta Mater. 45, 3283–3296.

Zhang, S., Karato, S., 1995. Lattice preferred orientation of olivine deformed in simple shear. Nature 375, 774–777.

Zhang, S., Karato, S., Fitz Gerald, J., Faul, U.H., Zhou, Y., 2000. Simple shear deformation of olivine aggregates. Tectonophysics 316, 133–152.